International Journal of Engineering, Science and Mathematics
Vol. 15 Issue 9,Sep 2026,
ISSN: 2320-0294 Impact Factor: 8.215
Journal Homepage: http://www.ijesm.co.in, Email: ijesmj@gmail.com
Double-Blind Peer Reviewed Refereed Open Access International Journal - Included in the International Serial Directories Indexed & Listed at: Ulrich's Periodicals Directory ©, U.S.A., Open J-Gage as well as in Cabell's Directories of Publishing Opportunities, U.S.A

STUDY OF RADIATIVE MHD NANOFLUID FLOW AND HEAT TRANSFER OVER AN INCLINED VERTICAL POROUS PLATE UNDER CONVECTIVE HEATING

Dhananjaiah D.S
Dept of Mathematics
Government First Grade College,K.R.Nagara
Mysuru,Karnataka,India.

Abstract

The radiative magneto hydrodynamic flow of a viscous, incompressible, electrically conducting non-Newtonian nanofluid over a vertically oriented porous surface that accelerates exponentially,Where a low magnetic Reynolds number is assumed to maintain a uniform magnetic field,and the effects of ramped temperature,heat absorption,and a first-order chemical reaction are included,with water serving as the base fluid containing silver (Ag) and titanium dioxide (TiO_2) nanoparticles combined with ethylene glycol to form the nanofluid,the results indicate that increasing nanoparticle volume fractions reduces the Nusselt number while heat absorption enhances it near the surface,and by applying similarity transformations,the governing nonlinear partial differential equations are converted into ordinary differential equations and solved numerically using the variational finite element method (FEM).

Keywords:MHD flow, Inclined plate, Magnetic field,FEM.

1.Introduction.

A nanofluid is a liquid that contains very tiny particles called nanoparticles, which are measured in nanometers. In heat transfer,these small particles are mixed with normal fluids to improve their performance. Common nanoparticles include metals like aluminum and copper, oxides such as Al_2O_3 and CUO, carbides like SiC, nitrides like AIN and SiN, and nonmetals such as graphite and carbon nanotubes.

Nanoparticles usually have a size between 1 and 100 nanometers. To improve heat transfer, nanofluids generally contain up to 5% nanoparticles by volume. These particles are added to liquid to increase their thermal conductivity. Many studies have been carried out to understand and improve this property. Choi [1] first introduced the concept of nanofluids while working on advanced cooling systems. Research by Eastman [4] and others showed that adding 5% CuO nanoparticles to water can increase its thermal conductivity by up to 60%. This happens because nanoparticles increase the surface area inside the fluid. Additionally, Eastman et al. [5] demonstrated that adding copper nanoparticles with a volume proportion of less than 1% to ethylene glycol or oil enhanced the thermal conductivity by 40%. According to Choi et al. [2], adding carbon nanotubes to ethylene glycol or oil increases heat conductivity by 150%. Furthermore, Xie et al. [8] found that adding alumina nanoparticles increases the thermal conductivity of an Al2O3-based nanofluid based on ethylene glycol by 25–30%. This kind of increase in thermal conductivity depends on a number of different mechanisms, including particle size, agglomeration, volume fraction, Brownian motion, thermophoresis, and more, in addition to the higher thermal conductivity characteristics of the added nanoparticles. Numerous studies that address the mass transfer and heat properties of nanofluids by taking thermophoresis effects and Brownian motion into consideration can be found in the literature.

The Cheng-Minkowycz problem related to natural convection boundary-layer flow in a porous medium filled with nanofluid has recently been examined by Nield and Kuznetsov.[7] Khan and pop [6] also studied the boundary-layer flow of a nanofluid over a strectching sheet.Additionally,Chamkha at el [3] and his co-authors investigated mixed convection magnetohydrodynamic flow of a nanofluid over a stretching permeable surface,considering the effects of Brownian motion and thermophoresis.

To the best of the authors knowledge, no previous studies have addressed the MHD mixed convection heat and mass transfer characteristics of a porous medium saturated with nanofluid over an inclined vertical flat plate. Especially when thermal radiation and heat generation pr absorption are taken into account. Therefore, this work focuses on discussing this particular problem.

2.Formulation of the problem

This study looks at a steady, smooth two –dimensional flow of a nanofluid over a very long tilted flat plate. The plate is placed in a porous material filled with nanofluid and is inclined at a small angle α from the vertical position.

The nanofluid model takes into account two important effects random movement of particles and movement caused by temperature differences. In this setup, the x-direction is along the surface of the plate, while they-direction is perpendicular to it, moving into the fluid. The plate surface is kept at a constant temperature $T_{w.}$ and concentration $C_{w.}$.These values are higher than the surrounding fluids temperature T_∞ and concentration C_∞.Based on these conditions, the governing equations are formed.

$$\frac{\partial u}{\partial x}+\frac{\partial v}{\partial y}=0$$

(1.1)

$$\frac{\partial p}{\partial y}=0$$

(1.2)

$$\mu_f\frac{1}{\kappa}u=-\frac{\partial p}{\partial x}+g\left[(1-C_\infty)\rho_{f\infty}\beta(T-T_\infty)-\left(\rho_p-\rho_{f\infty}\right)(C-C_\infty)\right]\cos\alpha-\frac{\sigma\beta_o^2}{\rho_f}u$$

(1.3)

$$\left(u\frac{\partial T}{\partial x}+v\frac{\partial T}{\partial y}\right)=\frac{k_m}{(\rho c)_f}\frac{\partial^2 T}{\partial y^2}+\frac{(\rho c)_p}{(\rho c)_f}\left[D_B\frac{\partial C}{\partial y}.\frac{\partial T}{\partial y}+\left(\frac{D_T}{T_\infty}\right)\left(\frac{\partial T}{\partial y}\right)^2\right]-Q(T-T_\infty)-\frac{1}{(\rho c)_f}.\frac{\partial}{\partial y}(q_r)(1.4)$$

$$\frac{1}{\varepsilon}\left(u\frac{\partial C}{\partial x}+v\frac{\partial C}{\partial y}\right)=D_B\frac{\partial^2 C}{\partial y^2}+\left(\frac{D_T}{T_\infty}\right)\frac{\partial^2 T}{\partial y^2}$$

(1.5)

The bc's are:

$$u=0,\quad T=T_w,\quad C=C_w\ at\ y=0$$

(1.6)

$$u=u_\infty,\quad T\longrightarrow T_\infty,\quad C\longrightarrow C_\infty\ at\ y=\infty$$

(1.7)

p may be eliminated from Equation (1.2) and (1.3) by cross-differentiation and the continuity equation (1.1) will be satisfied introducing a stream function ψ defined by the Cauchy-Riemann equations:

$$u=\frac{\partial\psi}{\partial y},\qquad v=-\frac{\partial\psi}{\partial x}$$

(1.8)

By substituting Eqn (1.8) in Eqs (1.3), (1.4), (1.5), we arrive at the following three coupled similarity equations:

$$\frac{\partial^2\psi}{\partial y^2}=\left[\frac{(1-C_\infty)\rho_{f\infty}\beta gk}{\mu}\frac{\partial T}{\partial y}-\frac{\left(\rho_p-\rho_{f\infty}\right)gk}{\mu}\frac{\partial C}{\partial y}\right]\cos(\alpha)-\frac{\sigma\beta_o^2}{\rho}u$$

(1.9)

$$\frac{\partial\psi}{\partial y}\frac{\partial T}{\partial x}-\frac{\partial\psi}{\partial x}\frac{\partial T}{\partial y}=\frac{k_m}{(\rho c)_f}\frac{\partial^2 T}{\partial y^2}+\frac{\varepsilon(\rho c)_p}{(\rho c)_f}\left[D_B\frac{\partial C}{\partial y}\frac{\partial T}{\partial y}+\left(\frac{D_T}{T_\infty}\right)\left(\frac{\partial T}{\partial y}\right)^2\right]-Q(T-T_\infty)-\frac{1}{(\rho c)_m}\frac{\partial}{\partial y}(q_r)$$

(1.10)

$$\frac{1}{\varepsilon}\left(\frac{\partial\psi}{\partial y}\frac{\partial C}{\partial x}-\frac{\partial\psi}{\partial x}.\frac{\partial C}{\partial y}\right)=D_B\frac{\partial^2 C}{\partial y^2}+\left(\frac{D_T}{T_\infty}\right)\frac{\partial^2 T}{\partial y^2}$$

(1.11)

The following similarity transformations are introduced to simplify the mathematical analysis of the problem

$$\eta=\frac{y}{x}Pe_x^{1/2},\ f(\eta)=\frac{\psi}{\alpha_m Pe_x^{1/2}}\ ,\ \theta(n)=\frac{T-T_\infty}{T_w-T_\infty}\qquad \phi(n)=\frac{C-C_\infty}{C_w-C_\infty} \tag{1.12}$$

where, $\alpha_m=\frac{k_m}{(\rho c)_f}$.

By using Rosseland approximation for radiation, the radiative heat flux q_r is defined as

$$q_r=-\frac{4\sigma^*}{3K^*}\frac{\partial T^4}{\partial y},$$

(1.13)

whereσ^* is the Stephan-Boltzman constant

K^* is the mean absorption coefficient

We assume that the temperature differences within the flow are such that the term T^4 may be expressed as a linear function of temperature. This is accomplished by expanding T^4 in a Taylor series about a free stream temperature T_∞ as follows:

$$T^4=T_\infty{}^4+4T_\infty{}^3(T-T_\infty)+6T_\infty{}^2(T-T_\infty)^2+\cdots$$

(1.14)

Neglecting higher-order terms in the above Eq. (19) beyond the first degree in$(T-T_\infty)$, we get

$$T^4\cong\ 4T_\infty{}^3T-3T_\infty{}^4\ .$$

(1.15)

Thus substituting Eq. (20) in Eq. (18), we get

$$q_r=-\frac{16T_\infty{}^3\sigma^*}{3K^*}\frac{\partial T}{\partial y}.$$

(1.16)

Momentum boundary layer equation:

$$f'' = \frac{Ra_x}{Pe_x}(\theta' - Nr\,\varphi')Cos(\alpha) + Mf' \tag{1.17}$$

Thermal boundary layer equation:

$$\left(1 + \frac{4}{3}An\right)\theta'' + \frac{1}{2}\,f\,\theta' + Nb\,\theta'\varphi' + Nt(\theta')^2 - Q\theta = 0 \tag{1.18}$$

Concentration (species diffusion) boundary layer equations:

$$\varphi'' + \frac{1}{2}\,Le\,\varphi' + \frac{Nt}{Nb}\theta'' = 0 \tag{1.19}$$

The transformed bc's are

$$\eta = 0,\quad f = 0\,,\ \theta = 1\,,\quad \phi = 1.\eta \longrightarrow \infty,\ f' = 1\,,\ \theta = 0\,,\quad \phi = 0. \tag{1.20}$$

where a prime denotes differentiation with respect to η, and the key thermophysical parameters dictating the flow dynamics are defined by

$$Nr = \frac{(\rho_p - \rho_{f\infty})(C_w - C_\infty)}{\rho_{f\infty}\beta(T_w - T_\infty)(1 - C_\infty)},$$

$$Nb = \frac{\varepsilon\beta(\rho c)_p D_B(C_w - C_\infty)}{(\rho c)_f\ \alpha_m}, Nt = \frac{\varepsilon(\rho c)_p D_T(T_w - T_\infty)}{(\rho c)_f\ \alpha_m T_\infty}$$

$$Le = \frac{\alpha_m}{\varepsilon D_B},\ Ra_x = \frac{(1 - C_\infty)Kg\beta\rho_{f\infty}(T_w - T_\infty)x}{\mu\alpha_m}\ ,\ \ Pe_x = \frac{U_\infty x}{\alpha_m},$$

$$Ra = \frac{Ra_x}{Pe_x},\qquad Q = \frac{x^2}{Pe_x\alpha_m},\qquad An = \frac{4T_\infty{}^3\sigma^*}{K^*\alpha_m},\qquad M = \frac{\sigma\beta_o^2 x}{\rho Pe_x{}^{1/2}}.$$

Where Le, Nr, Nb, Nt, Ra_x, Pe_x, M, Q and An are Lewis number, buoyancy ratio parameter, Brownian motion parameter, thermophoresis parameter, local Darcy-Rayleigh number, local Peclet number, magnetic field parameter.

Heat generation/absorption parameter and thermal radiation parameter respectively. We note that porosity (ε) is absorbed into the Nb, Nt and Le parameters, and therefore it is not explicitly simulated in this study. Quantities of practical interest in this problem are the local Nusselt number Nu_x, and the local Sherwood number Sh_x, are defined as

$$Nu_x = \frac{xq_w}{k(T_w - T_\infty)} Sh_x = \frac{xq_m}{D_B(C_w - C_\infty)} \tag{1.21}$$

$$(Pe_x)^{-1/2}Nu_x = -\theta'(0),\ (Pe_x)^{-1/2}Sh_x = -\phi'(0), \tag{1.22}$$

The set of ordinary differential equations (1.17) – (1.19) are highly non-linear, and therefore cannot be solved analytically. The finite-element method has been implemented to solve these non-linear equations.

The very important aspect in this numerical procedure is to select an approximate finite value of η_∞. So, in order to estimate the relevant value of η_∞, the solution process has been started with an initial value of $\eta_\infty = 4$, and then the equations (1.17) – (1.19) are solved together with boundary conditions (1.20). We have updated the value of η_∞ and the solution process is continued until the results are not affected with further values of η_∞.The choice of $\eta_{max} = 8$ *and* $\eta_{max} = 5$for temperature and concentration have confirmed that all the numerical solutions approach to the asymptotic values at the free stream conditions.

3. Solution of the problem

The effective properties of hybrid nanofluids are established by hybrids theory and phenomenon commandments. The renowned empirical correlation foranofluid is specified as follows

$$\rho_{hnf} = (1-\phi_2)\left[(1-\phi_1)_{\rho f} + \phi_1\rho_{s_1}\right] + \phi_2\rho_{s_2}, \mu_{hnf} = \frac{\mu_f}{(1-\phi_1)^{2.5}(1-\phi_2)^{2.5}},$$
$$\sigma_{hnf} = \sigma_{bf}\left[\sigma_{s_2}(1+2\phi_2) + 2\sigma_{bf}(1-\phi_2)\sigma_{s_2}(1-\phi_2) + \sigma_{bf}(2+\phi_2)\right],$$
$$\sigma_{bf} = \sigma_f\left[\sigma_{s_1}(1+2\phi_1) + 2\sigma_f(1-\phi_1)\sigma_{s_1}(1-\phi_1) + \sigma_f(2+\phi_1)\right],$$
$$(\rho\beta_T)_{hnf} = (1-\phi_2)\left[(1-\phi_1)(\rho\beta_T)_f + \phi_1(\rho\beta_T)_{s_1}\right] + \phi_2(\rho\beta_T)_{s_2},$$
$$(\rho\beta_C)_{hnf} = (1-\phi_2)\left[(1-\phi_1)(\rho\beta_C)_f + \phi_1(\rho\beta_C)_{s_1}\right] + \phi_2(\rho\beta_C)_{s_2},$$
$$(\rho C_p)_{hnf} = (1-\phi_2)\left[(1-\phi_1)(\rho C_p)_f + \phi_1(\rho C_p)_{s_1}\right] + \phi_2(\rho C_p)_{s_2},$$
$$k_{hnf} = k_{bf}\left[\frac{k_{s_2} + 2k_{bf} - 2\phi_2(k_{bf} - k_{s_2})}{k_{s_2} + 2k_{bf} + \phi_2(k_{bf} - k_{s_2})}\right], k_{bf} = k_f\left[\frac{k_{s_1} + 2k_f - 2\phi_1(k_f - k_{s_1})}{k_{s_1} + 2k_f + \phi_1(k_f - k_{s_1})}\right],$$
$$D_{hnf} = (1-\phi_1)(1-\phi_2)D_f$$

where$\phi_1 = 0$ (exclusive of suspension of silver nanoparticles) represents titania/ H_2O and ethylene glycol (Casson) nanofluids and $\phi_2 = 0$ (exclusive of suspension of TiO_2 nanoparticles) represents TiO_2/H_2O and ethylene glycol nanofluid. Both $\phi_1 = 0 = \phi_2$ correspond to the base fluid (H_2O and ethylene glycol). The thermophysical properties of water and ethylene glycol and solid nanoparticles (Agand TiO_2). we acquire the solutions for the velocity distribution, temperature and concentration distributions after moving on the t-direction for the flow near a vertical surface with the ramped plate temperature specified as

$$q(z,t) = q_1(z,t) - H(t-1)q_1(z,t-1)$$
$$\theta(z,t) = f_1(\alpha_2, a_5, t) - H(t-1)f_1(\alpha_3, a_5, t-1)$$
$$\phi(z,t) = f_1(\alpha_3, \mathrm{Kr}, t)$$

To emphasize the consequence of the ramped wall temperature on the flow field, this may be consequential to contrast such a nanofluid flow due to the uniform wall temperature. $\theta(0,t) = 1$, for $t = 0$. Under the assumptions portrayed in this present paper, it is revealed that the temperature distribution and velocity fields for the flow over a surface by the uniform wall temperature may be articulated as follows.

$$q(z,t) = q_2(z,t)$$
$$\theta(z,t) = f_7(\alpha_1, a_5, 0, t)$$

The velocity and temperature distribution for the uniform wall temperature and the time-altering concentration distribution, respectively.

For engineering aspects, the non-dimensional shear stresses due to the primary and secondary flow near the plate ($z = 0$).

For the ramped wall temperature

$$\tau = \tau_x + i\tau_y = \left(\frac{\partial q}{\partial z}\right)_{z=0} = q_3(t) - H(t-1)q_3(t-1)$$

For the uniform wall temperature

$$\tau = \tau_x + i\tau_y = \left(\frac{\partial q}{\partial z}\right)_{z=0} = q_4(t)$$

The Nusselt number in terms of rate of heat transport near the plate surface ($z = 0$)

$$\theta'(0,t) = -\left(\frac{\partial \theta}{\partial z}\right)_{z=0} = -\sqrt{a_4}\big(g_1(a_5,t) - H(t-1)g_1(a_5,t-1)\big)$$
$$\theta'(0,t) = -\left(\frac{\partial \theta}{\partial z}\right)_{z=0} = -\sqrt{a_4}g_7(a_5,0,t)$$

The Sherwood number in terms of rate of mass transport near the plate surface ($z = 0$)

$$\phi'(0,t) = -\left(\frac{\partial \phi}{\partial z}\right)_{z=0} = -\sqrt{a_{10}}g_1(\mathrm{Kr},t)$$

4.Analysis of the numerical results

Nanofluids can be prepared using two methods single step and two step techniques. The single step method is mainly used for producing hybrid nanofluids on a small scale, while the second is suitable for mass production. The present study considers an unsteady MHD Darcy flow of an incompressible viscous electrically conducting non-Newtonian casson hybrid nanofluid over an infinite, exponentially accelerated vertical surface, including the effects of slip velocity and a rotating frame, along with Hall and ion slip effects. A water and ethylene glycol mixture is used as the base fluid. The exact solutions of the governing equations are obtained using the laplace transform method. The flow is analyzed with respect to various non-dimensional parameters that describe its characteristics, and the results are presented in graphical and tabular form. Selected graphical profiles are shown in figs 2.1 to 2.4.

Figures 2.1 and 2.2 show how the magnetic field parameter (M) affects the temperature and concentration patterns in the boundary layer. It is evident from these pictures that as M increases, so does the thickness of the thermal and solutal boundary layers. This is due to the fact that a magnetic field in an electrically conducting fluid creates a force known as the Lorentz force, which acts against the direction of flow and degrades velocity profiles. At the same time, the fluid must exert additional effort to overcome the drag force imposed by the Lorentzian retardation; this additional effort can be transformed into thermal energy, which raises the fluid's temperature (Fig.2.1), and it also raises the concentration profiles (Fig.2.2).

Figures 2.3 and 2.4 show how the temperature and concentration profiles change for various plate inclination angle (α) values. Figure 2.4 illustrates how an increase in the plate inclination angle (α) makes the fluid oppose its travel and raises its temperature (Fig.2.3).

As the value of α increases, the concentration distribution also increases, as shown in fig 2.4. When α increases, the buoyancy ratio in the momentum equation decreases, Which causes the temperature and concentration to rise. For a vertical plate $\alpha = 0$, the buoyancy force is maximum. However, for a horizontal plate $\alpha = \pi/2$, the buoyancy force becomes zero because the term disappears. From fig 2.4 it is clear that increasing the inclination angle α increases both the thermal and concentration boundary layers.

5.Graphs

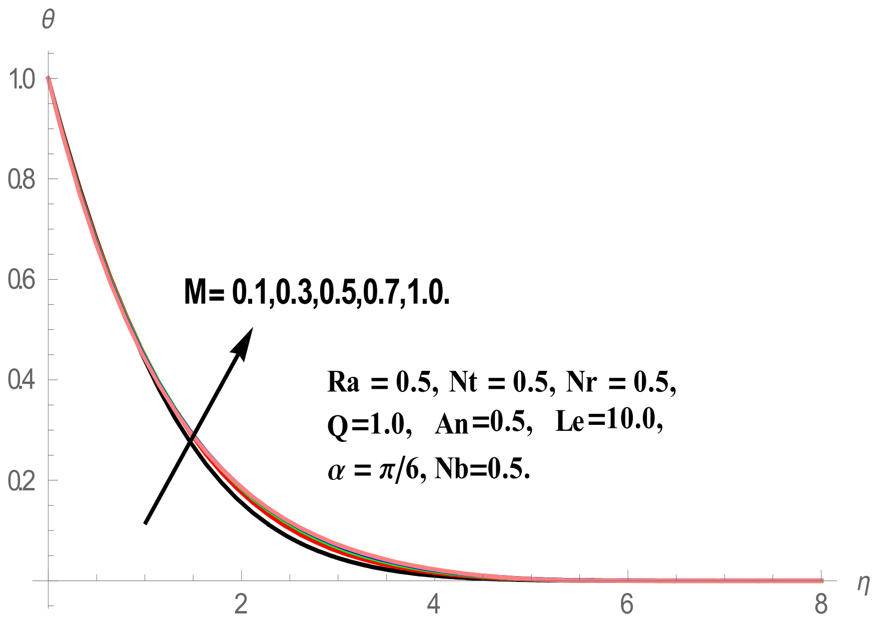

Fig.2.1. Temperature profiles for different values of M.

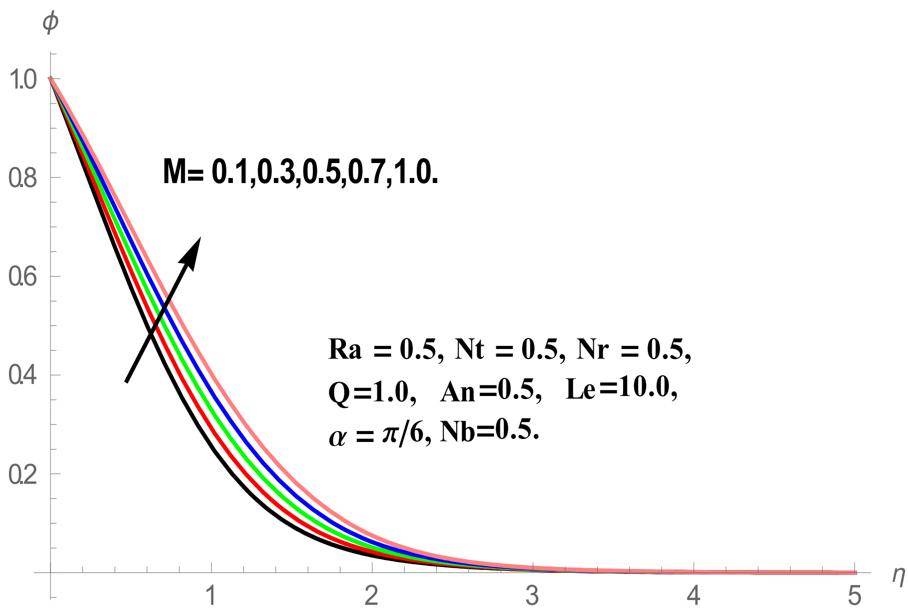

Fig.2.2. Concentration profiles for various values of M.

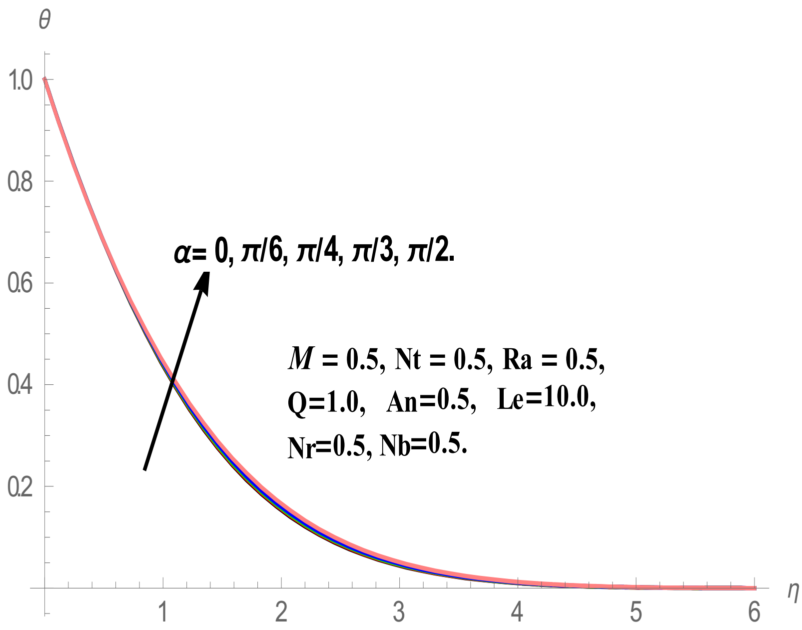

Fig.2.3. Temperature profiles for different values of α.

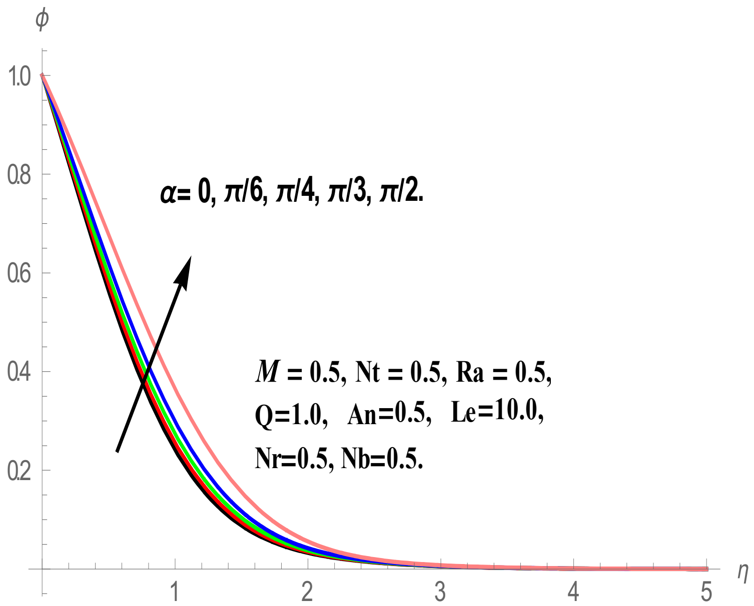

Fig.2.4. Concentration profiles for different values of α.

6.Numerical values

The data in Table 3.1 shows how the reduced Nusselt number and Sherwood number change when the prandtl number (Pr), Brownian motion parameter (Nb), and buoyancy parameter (Nr) are varied, While other values stay constant.

When Pr increases, both the reduced Nusselt and Sherwood numbers also increase for all values of Nb and Nr. However, if Pr is kept constant, increasing Nb or Nr causes both numbers to decrease. Table 3.2 explains the effect of the Lewis number. As the Lewis number increases, the reduced Nusselt increases slightly, but the reduced Sherwood number increases significantly.

The data in Table 3.1 indicate how the reduced Nusselt and Sherwood numbers are affected by the changes in the Prandtl number Pr, the Brownian motion parameter Nb and the buoyancy parameter Nb when the rest of the parameters are fixed at the values indicated in the table heading. For every combination of Nb and Nr, both the reduced Nusselt and reduced Sherwood numbers increase with the increase in Pr. For a fixed Pr, both the reduced Nusselt number and the reduced Sherwood number decrease as Nb and Nr each increase. Table 3.2 allows the reader to see how the changes in the Lewis affect the reduced Nusselt number and the reduced Sherwood number. As the Lewis number increases the reduced Nusselt number increases slightly but there is a substantial increase in the reduced Sherwood number. Tables.3.1 and 3.2 provide information about the heat and mass transfer characteristics of the flow in a form convenient for research and engineering calculations.

We also noticed from Table. 3.1 that the Sherwood number (Sh) enhances as Schmidt number (Sc) and time t increase. The Nusselt number (Nu) increases with Prandtl number (Pr) and decreases with radiation conduction parameter (R) and time (t) (Table.3.2). The skin friction components τx and τy enhance with increasing Prandtl number (Pr) and decrease with thermal Grashof number (Gr) and mass Grashof number (Gm). The component τx increases,and τy decreases, as Hartmann number (M) and permeability parameter (K) increase, whereas the reverse behavior is observed with increasing Sc, radiation conduction parameter (R), and frequency of oscillation ωt (Table.3.3).

Table.3.1. Variation of Nu and Sh with Pr, Nb and Nr for Nt= 0.1, Nc = 10 and Le = 10.

N_b	N_r	P_r=1		P_r=5		P_r=10	
		Nu	Sh	Nu	Sh	Nu	Sh
0.1	0.1	0.5816	0.8328	0.5243	1.3012	0.1266	1.41343
	0.2	0.5784	0.8197	0.5209	1.2881	0.123	1.40043
	0.3	0.5751	0.8059	0.5172	1.2744	0.1193	1.38683
	0.4	0.5717	0.7914	0.5135	1.2601	0.1155	1.37253
	0.5	0.5681	0.7762	0.5095	1.2451	0.1115	1.35763
	0.6	0.5642	0.76	0.5054	1.2292	0.1073	1.34193
	0.7	0.5602	0.7427	0.501	1.2124	0.1028	1.32533
	0.8	0.5389	0.8935	0.4776	1.3631	0.0787	1.47573
0.3	0.1	0.5369	0.8817	0.4752	1.3515	0.0763	1.46433

	0.2	0.5346	0.8695	0.4728	1.3396	0.0738	1.45243
	0.3	0.5322	0.8567	0.4702	1.3271	0.0712	1.44013
	0.4	0.5298	0.8434	0.4676	1.3141	0.0685	1.42733
	0.5	0.5273	0.8294	0.4649	1.3006	0.0658	1.41393
	0.6	0.5247	0.8147	0.462	1.2864	0.0629	1.39993
	0.7	0.5219	0.7991	0.459	1.2715	0.0599	1.38523
	0.8	0.498	0.9084	0.4325	1.3793	0.0324	1.49243
0.5	0.1	0.4963	0.8971	0.4305	1.3682	0.0305	1.48143
	0.2	0.4945	0.8853	0.4286	1.3567	0.0285	1.47003
	0.3	0.4927	0.873	0.4266	1.3448	0.0265	1.45823
	0.4	0.4908	0.8602	0.4245	1.3324	0.0244	1.44603
	0.5	0.4888	0.8467	0.4224	1.3194	0.0222	1.43323
	0.6	0.4868	0.8327	0.4201	1.3059	0.0199	1.41993
	0.7	0.4846	0.8178	0.4178	1.2918	0.0176	1.40603
	0.8	0.245	-0.15	0.147	0.253	-0.262	0.34623

Table.3.2. Variation of Nu and Sh with Le, Nb and Nr for Nt =0.1, Nc =10 and Pr=10.

N_b	N_r	Le = 1		Le = 5		Le = 10	
		Nu	Sh	Nu	Sh	Nu	Sh
0.1	0.1	0.3696	1.2404	0.4052	1.2928	0.612	1.5597
	0.2	0.3666	1.2278	0.4018	1.2802	0.6086	1.5472
	0.3	0.3634	1.2147	0.3984	1.2671	0.605	1.5342
	0.4	0.3601	1.2009	0.3947	1.2534	0.6013	1.5206
	0.5	0.3567	1.1864	0.391	1.2391	0.5975	1.5063
	0.6	0.3531	1.1712	0.387	1.2241	0.5935	1.4914
	0.7	0.3492	1.155	0.3829	1.2082	0.5893	1.4757
	0.8	0.3452	1.1377	0.3785	1.1914	0.5849	1.4591
0.3	0.1	0.3239	1.2885	0.3551	1.3421	0.5607	1.6095
	0.2	0.3218	1.2767	0.3527	1.3305	0.5583	1.5981
	0.3	0.3196	1.2645	0.3503	1.3186	0.5558	1.5862
	0.4	0.3172	1.2517	0.3477	1.3061	0.5532	1.5739
	0.5	0.3148	1.2384	0.3451	1.2931	0.5505	1.5611
	0.6	0.3123	1.2244	0.3424	1.2796	0.5478	1.5477

	0.7	0.3097	1.2097	0.3395	1.2654	0.5449	1.5337
	0.8	0.3069	1.1941	0.3365	1.2505	0.5419	1.519
0.5	0.1	0.283	1.3034	0.31	1.3583	0.5144	1.6262
	0.2	0.2813	1.2921	0.3081	1.3472	0.5125	1.6152
	0.3	0.2795	1.2803	0.3061	1.3357	0.5105	1.6038
	0.4	0.2777	1.268	0.3041	1.3238	0.5085	1.592
	0.5	0.2758	1.2552	0.302	1.3114	0.5064	1.5798
	0.6	0.2738	1.2417	0.2999	1.2984	0.5042	1.567
	0.7	0.2718	1.2277	0.2976	1.2849	0.5019	1.5537
	0.8	0.2696	1.2128	0.2953	1.2708	0.4996	1.5398

Table. 3.3: Skin friction

M	K	**Gr**	**Gm**	**Pr**	**Sc**	R	ωt	τ_x	τ_y
0.5	0.5	3	5	0.71	0.22	1	$\pi/6$	0.580552	0.053314
1								0.624001	0.042828
2								0.737663	0.033856
	1							0.860554	0.033556
	2							1.097547	0.025458
		5						0.426522	0.015852
		7						0.31652	0.009854
			7					0.401665	0.036826
			10					0.286485	0.026085
				3				0.764247	0.086779
				7				0.897985	0.142554
					0.3			0.501665	0.086827
					0.6			0.437585	0.127852
						2		0.335655	0.245823
						3		0.254254	0.454185
							$\pi/4$	0.370898	0.097989
							$\pi/3$	0.257258	0.255778

7.References

1.Choi S.U.S,Enhancing thermal conductivity of fluids with nanoparticles, developments and applications of non-Newtonian flows, in: D.A. Siginer, H.P. Wang (Eds.), FED—Vol. 231/MD, Vol. 66, The American Society of Mechanical Engineers, New York, pp. 99–105,(1995).

2.Choi. S.U.S, Zhang.Z.G, Yu.W, Lockwood.F.E and Grulke. E.A, Anomalous thermal conductivity enhancement in nano-tube suspensions, Appl. Phys. Lett. 79 , 2252–2254, (2001).

3.Chamkha. A.J, Aly.A.M andAl-Mudhaf.H, Laminar MHD mixed convection flow of a nanofluid along a stretching permeable surface in the presence of heat generation or absorption effects, Int. J. Microscale Nanoscale Thermal Fluid Transp. Phenom 2, Article 3, (2011).

4.Eastman. J.A, Choi. S.U.S, Li.S, Thompson.L.J.andLee.S, Enhanced thermal conductivity through the development of nanofluids, in: S. Komarneni, J.C. Parker, H.J. Wollenberger (Eds.), Nanophase and Nanocomposite Materials II, MRS, Pittsburg, PA, pp.3–11, (1997).

5.Eastman. J.A, Choi. S.U.S, Li.S, Yu. W and ThompsonL.J, Anomalously increased effective thermal conductivities of ethylene glycol-based nano-fluids containing copper nano-particles, Appl. Phys. Lett. 78, 718–720, (2001).

6.Khan. W. A, and Pop. I, Boundary-layer flow of a nanofluid past a stretching sheet, Int. J. Heat Mass Transfer 53, 2477–2483, (2010).

7.Nield.D.A, and Kuznetsov.A.V, The Cheng-Minkowycz problem for natural convection boundary-layer flow in a porous medium saturated by a nanofluid,Int. J. Heat Mass Transfer 52,5792–5795, (2009).

8.Xie.H,Wang.J,Xi.T,Liu.Y,Ai.F and Wu.Q,Thermal conductivity enhancement of suspensions containing nanosized alumina particles,J.Appl.Phys.91,4568-4572,(2002)